

# Numerical analysis of the effect of V-angle on flying wing aerodynamics

Zahir Amine<sup>1a</sup> and Omer Elsayed<sup>\*2</sup>

<sup>1</sup>Aerospace Engineer, Brussels, Belgium

<sup>2</sup>International University of Rabat, School of Aerospace Engineering, LERMA Lab., Campus UIR Parc Technopolis, Rocade, Rabat-Sale, 11100-Sala Al Jadida, Maroc

(Received July 28, 2022, Revised February 11, 2023, Accepted February 13, 2023)

**Abstract.** In current research work, the aerodynamics performance of a newly designed large flying V aircraft is numerically investigated. Three Flying V configurations, with V-angles of 50°, 70° and 90° that represent the minimum, moderate, and maximum configurations respectively, were designed and modeled to assess their aerodynamic performance at cruise flight conditions. The unstructured mesh was developed using ICEM CFD and Ansys-Fluent was used as an aerodynamic solver. The developed models were numerically simulated at cruise flight conditions with a Mach number equal to 0.15.  $K-\omega$  SST turbulence model was chosen to account for flow turbulence. The authors performed steady flow simulations. The results obtained from the experimentation reveal that the maximum main angle configuration of 90° had the highest  $C_{Lmax}$  value of 0.46 compared to other configurations. While the drag coefficient remained the same for all three configurations, the 50° V-angle configuration achieved the maximum stall angle of 35°. With limited stall delay benefits, the flying V possesses no sufficient stability, due to the flow separation detected at whole elevon and winglet suction side areas at AoA equal and higher than 30°.

**Keywords:** blended wing body; flying V; flying wing; fuselage-wing design; numerical analysis; V-angle

## 1. Introduction

In the past five decades, tube-and-wing configurations dominated the commercial aviation sector in general. B-47 aircraft is an excellent example of this type of configuration since it is loaded with a tubular fuselage, swept wing, rearmost empennage, and propulsion system which are mounted beneath the wing and attached with the pylons, Martinez-Val (2007). Recently, there is a revolution happening in the aeronautics and aviation fields, thanks to technological advancements made in these domains. When compared to the first flown modern jets, the efficiency of the aircraft has increased by 100% during this period, as declared by Martinez-Val *et al.* (2010) and Torenbeek (2007). On the other hand, manufacturers must be open-minded to adapt to the remarkable development expected in the upcoming decades. There is a 5% increase expected in total income passenger-kilometers. Further, the manufacturers must also be prepared to overcome the challenges in terms of environmental effects, noise pollution and meeting population demands, Martinez-Val *et al.* (2007). Thus, several pioneering design arrangements has been lately

\*Corresponding author, Assistant Professor, E-mail: Omer.almatbagi@uir.ac.ma

<sup>a</sup>Graduate Student, E-mail: amine.zahir@uir.ac.ma

recommended along with one goal i.e., reduction of direct operating costs per passenger and the number of flights. For instance, Bolsunovsky *et al.* (2001) concluded the possibility of attaining higher technical and cost-effective characteristics of FW configuration airplane as compared with conventional airplanes. FW is a tail-less fixed-wing airplane with no specific fuselage whereas the payload flight crew, fuel, and equipment are held inside the main wing structure. The researchers declared that the proposed alternative design is advantageous in different aspects since it has numerous attributes such as generated lift, seating people, and trimming the aircraft which are achieved by distinctive incorporated components. These outcomes decrease the wetted area for same payload and reduce the friction drag, one of the major drag elements during cruise flight. Additionally, Flying Wings can perform better since they are smaller in size compared to conventional fuselage-wing airplanes. In a nutshell, it is argued that the operational cost/seat per mile can be decreased to nearly 23%, while the passenger number can be increased to 750 with high-capability FW, as stated by Bolsunovsky *et al.* (2001). Additionally, Martinez-Val *et al.* (2008) emphasized the potential operation gain of FW with 300 passengers using the range equation, Torenbeek (2013). It is an established fact that range factor has enhanced the performance of aircraft by up to 100%. When it is introduced with FW, an additional 15-20% increase can be achieved. Benad (2015), at Technische Universitat Berlin, analyzed and modified the basic FW which was manufactured in cooperation with Future Project Office at Airbus GmbH (Hamburg, Germany). The new conceptually designed aircraft was called 'Flying V' owing to its clear V-shaped geometry. It features longitudinal and lateral controls by trailing the edge elevens. Further, the directional stability and control functions are ensured by winglets (or fins) that are added on wingtips and rudders respectively. Due to the unwanted pitch-down moment, it generates at low speeds excluding high lift devices. According to Berta (2018), two turbofan engines are positioned over the trailing edge of the wing near the best location of the aircraft i.e., a plane of symmetry. Flying V design has a twin cylindrical tube that helps in carrying the pressurization loads. This concept is different from the standard cabin design of Blended Wing Body (BWB) and typical FW that are unique compared to conventional cylindrical design, Torenbeek (2013). Based on the concerns raised and top requirements, the new design is aimed at providing the best efficiency in aerodynamics with minimal weight to overcome the challenges in existing conventional commercial aircraft, A350-900. Further, the design also aims at achieving an equivalent minimal range of 14,350 km, a service ceiling of 13,100 m, a cruise Mach number of 0.85, and a passenger capability of 400-440 passengers. Because A350-900 performance data is not accessible due to which NASA Common Research Model (CRM), Vassberg (2008) is considered as a baseline model for comparison.

In the progress of developing a new comfortable and aerodynamically efficient flying-V aircraft design, Vink *et al.* (2020), reported that four aircraft interior models were created and a 1:1 scale mock-up was made for the Flying V interior. This was shown at a KLM 100-year event. 1692 guests of the mock-up handed their remarks from likely commuters were gathered on the chosen models giving feedback for additional improvement. Similarly, Rubio and Vos (2020) examined forty different engine locations to build an alternate model that estimates the aircraft's lift-to-drag ratio based on the location of the engine. Their findings show that mispositioning the engine results in a considerable lift-to-drag ratio loss of up to 55% when compared with the ideal integration configuration. Also, Wei *et al.* (2022) proposed a fast aerodynamic optimization technique for flying wing aircraft conceptual design. This method is intended to reduce the induced drag at the design point by adapting the camber and twist angle of the spanwise airfoil. Their results revealed that the coefficient of induced drag decreased by 10%, the pitching moment

coefficient decreased by an order of magnitude, and the lift drag ratio improved from 26.3 to 27.3. Recently the Flying-V aerodynamics and structures consideration were analyzed by Oosterom and Vos (2022). This research aims at the possibility of generating a family of Flying-V aircraft, which is a key stage in passenger aircraft progress presenting multiple aircraft alternatives at limited development and production expense. In the conceptual design phase of 'flying V', the weight is approximated. Further, vortex lattice methods and empirical correlations are used for the drag calculation. The model appears to be significantly encouraging with a 10% increase in the lift-to-drag ratio, a satisfactory benefit in terms of weight and drag as declared by Benad (2015).

Flow control over flying wing aircraft was investigated extensively in recent times. He *et al.* (2021) examined numerically and experimentally the efficiency of a passive gust alleviation device (PGAD) installed in a flying-wing aircraft with a 62.3 m wingspan at a large swept-back angle. The gust response dominated by the first three modes of the flying wing was extremely significant in the frequency at the first bending mode of the wing. The influence of cross-section configuration on the stress distribution and aeroelastic behavior of a flying wing aircraft was investigated by Sayed *et al.* (2022). The results reveal that various wing cross-section designs influence stress distribution as well as the aeroelastic stability of the aircraft. Additionally, the design with a smaller amount of stress strangulation is correlated with a higher flutter speed structure. A longitudinal aerodynamic control technology based on circulation control (CC) using trailing-edge synthetic jet actuators was suggested by Zhao *et al.* (2022). Results show that synthetic jets can enhance the lift, drag, and nose-down moment, with an ability of flight control at all angles of attack range. Meng *et al.* (2020) revised the advancement of static aeroelastic effect estimation and correction techniques for aircraft, with the damage and protection of aeroelastic. Likewise, they presented the static aeroelastic prediction and correction method, the widely practiced K-value method. To delay the position of vortex breakdown and improve the lift qualities of the flying wing aircraft, the vortex breakdown qualities of a flying wing aircraft under jet flow control were investigated numerically by Zhu *et al.* (2022). They concluded that the periodic energy injection can increase the peak value characteristics of the main frequency, increase the frequency range of the downstream flow field development, and speed up the rotation of the flow field next to the vortex breakdown. The ground proximity effect on the aerodynamic properties of the Flying V was numerically predicted by Ankith (2020). Simulations reveal an 11% decrease in the drag polar of the Flying V at the ground proximity when compared to unbounded flow.

Recently, an operational safety criterion has been numerically investigated between Flying V criteria and Airbus A350-900 via the cellular automata model by Gebauer, Julia, and Justus Benad (2021). The comparison results reveal that a shorter V-shaped cabin has more advantages than a longer conventional cabin. On the other hand, when passengers have to evacuate from a V-shaped cabin to one side of the aircraft, it seems to be disadvantageous for them. These are only initial predictions whereas further detailed calculations are necessary to evaluate the practicability of Flying V and verify the preliminary evaluations. Therefore, the current work investigates the aerodynamics of flying V aircraft and possible performance improvement by changing the main V-angle. Multiple configurations with different V-angles are designed and aerodynamic analysis is conducted to compare the lift and drag, generated by each geometry. This is a pioneering study in the overall analysis of the newly designed large flying V configuration. It is essential to keep in mind that the design of tailless aircraft requires compact integration of various parts than the conventional fuselage-wing design. Although the current research is related to aerodynamic characteristics, structural concerns, and limitations are studied from the initial phase.

Table 1 Characteristics of different NACA Airfoil sections

Airfoil section	$C_{lmax}$ ( $Re=3.10^6$ )	$\alpha(^{\circ})$	$C_{mo}$	$(C_l/C_d)_{max}$	$C_{ld}$	$C_{dmin}$	$(t/c)_{max}$
NACA 0009	1.25	13	0	39	0	0.0052	9%
NACA 4410	1.5	13	-0.09	71	0.4	0.006	10%
NACA 2411	1.4	14	-0.05	86	0.3	0.0065	11%

## 2. Physical and numerical setup, mesh generation

This section explains the physical and numerical setups used for aerodynamic analysis and mesh generation with different parameters.

### 2.1 Airfoil choice

In airfoil selection, several criteria need to be assessed. According to Sadraey (2012), the crucial criteria are as follows; design lift coefficient ( $C_{ld}$ ), maximum lift coefficient ( $C_{lmax}$ ), minimum drag coefficient ( $C_{dmin}$ ), lift-to-drag ratio ( $(C_l/C_d)_{max}$ ), lift curve slope, pitching moment coefficient ( $C_m$ ), appropriate stall condition and easy cost-effective manufacturability. Further, a few additional design conditions must also be considered. For example, if a fuel tank is allocated within the inboard section of the wing, then the airfoil should permit it with an appropriate room. For high-speed aircraft with low lift requirements (as in the case of high subsonic conventional aircraft), the typical wing  $(t/c)_{max}$  should be between 9% and 12%. In this background, the current study compares three airfoil candidates to make a reasonable choice, and table 1 shows the characteristics of each airfoil.

Based on the evaluation of values cited in Table 1, it can be concluded that:

- NACA0009 has the greatest speed because it has the smallest ( $C_{dmin}=0.0052$ ).
- NACA2411 has the smallest stall speed since it has the highest stall angle ( $14^{\circ}$ ).
- NACA2411 possesses the maximum endurance since it has the highest  $(C_l/C_d)_{max}$ .
- NACA2411 delivers a low  $C_{mo}$  which translates to less control problems during flight.
- And finally, the  $(t/c)_{max}$  of NACA2411 is within the range of typical  $(t/c)_{max}$  for high subsonic passenger aircraft, Sadraey (2012).

Based on the outcomes briefed above, the NACA2411 airfoil is selected for the 'Flying wing' design. For this wing design, three airfoil sections are required of variable chord lengths and thicknesses. For the winglets' design, a blended winglet type is chosen to reduce the induced drag component which consequently reduces fuel consumption. This in turn reduces the emission of  $CO_2$  and  $NO_x$  too and mitigates noise pollution. In addition to the above, both ranges as well as the payload can be increased.

### 2.2 Flying V Configuration

Three Flying V configurations are investigated with three different main V-angles such as the lowest angle possible for flying V ( $50^{\circ}$ ), the maximum possible angle ( $90^{\circ}$ ), and a moderate angle value ( $70^{\circ}$ ). When all three configurations are critically assessed, it provides a bird's eye view of the performances that can be changed with variants of the main V-angle. Fig. 1 (a)-(c) shows an overview and dimensions of three 'flying V' configurations.

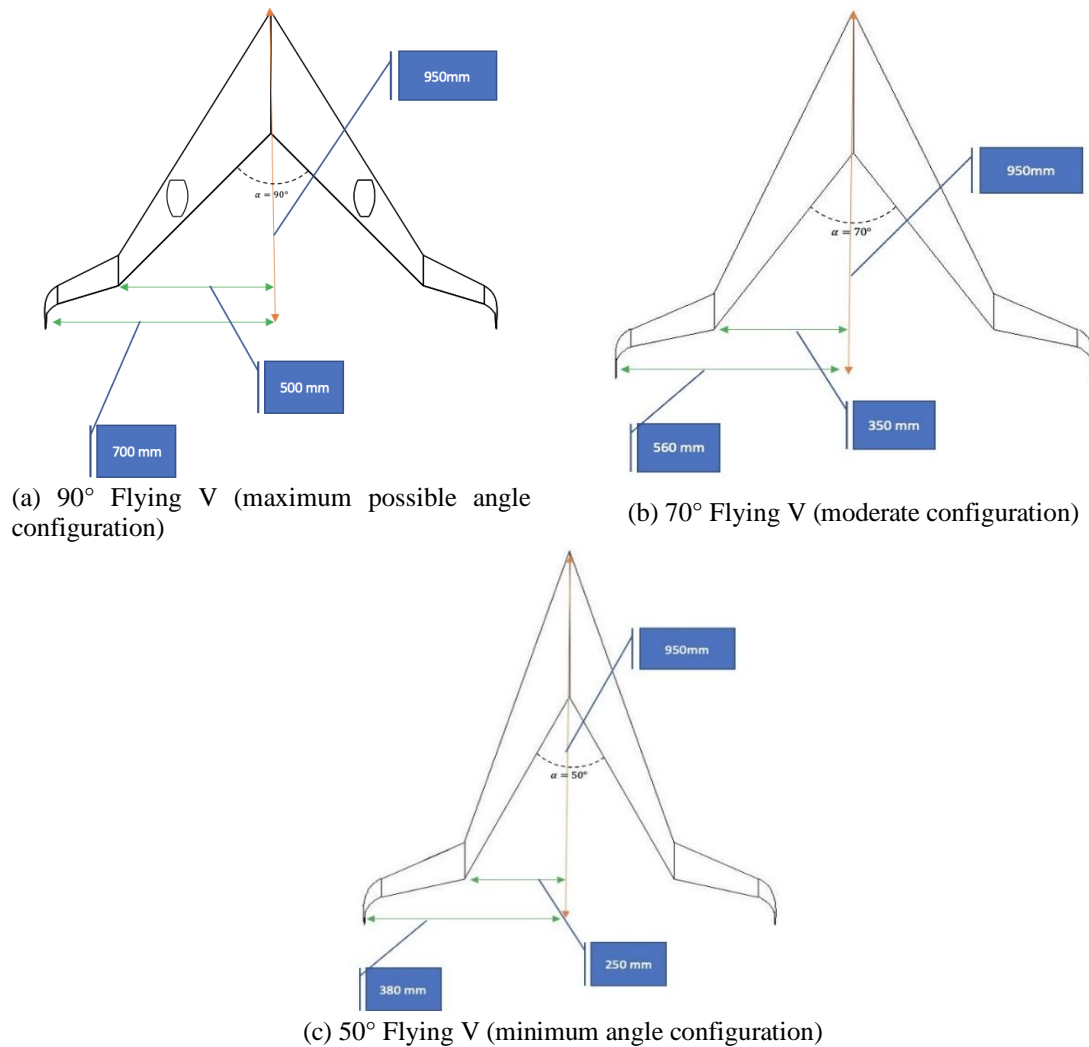


Fig. 1 Dimensions of the 90°, 70°, and 50° Flying V configurations

### 3. Grid generation

#### 3.1 Unstructured grid generation

The type of grid and its quality play a relevant role in numerical simulations. In current research work, the tetrahedral unstructured mesh is produced using ICEM CFD meshing tool. Fig. 2(a) shows the dimensions used for the computational domain and the boundary conditions assigned to each face whereas the ‘flying V’ meshing view is shown in Fig. 2(b).

#### 3.2 Grid convergence study

A grid independence study is conducted to ensure that the results obtained are final and

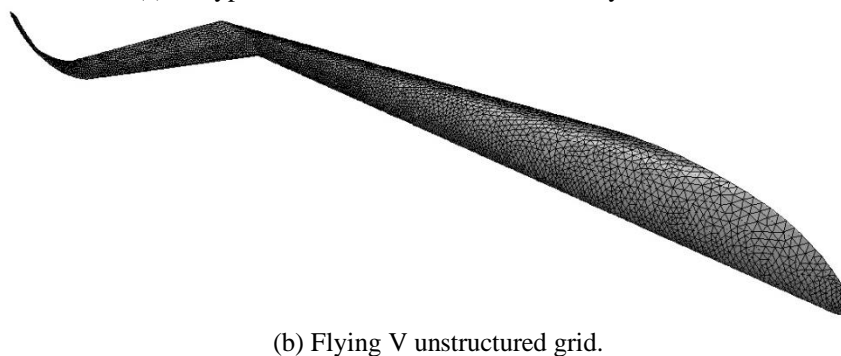
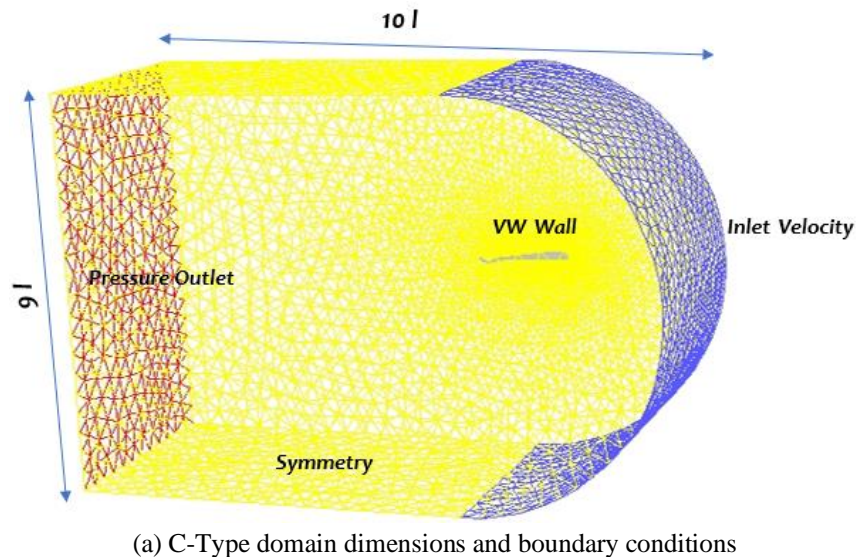


Fig. 2 C-Type domain dimensions (a) and Flying V unstructured grid (b)

independent of mesh so that in case of any further refinement in mesh size, it does not produce better results. Fig. 3 compares the variations in lift and drag coefficients and the number of mesh elements in millions. Lift and drag coefficients' curves reveal that after 3 million mesh elements, no significant change and further refinement are needed. At high curvature areas, for instance, at the leading and trailing edges of the wing, grid clustering is needed. Moreover, according to Chan *et al.* (2002), it is advised to approximate the element size of the surface grid based on the local chord. With a 0.1% sized local chord, present near the leading edge, it is sufficient enough to accurately define the flow changes.

### 3.3 Validation

Aerodynamic analysis was validated through experimental measurement values obtained for Onera M6 wing.

#### 3.3.1 Onera M6 wing

Onera M6 Wing is used as a benchmark for numerical setup validation. It represents a good

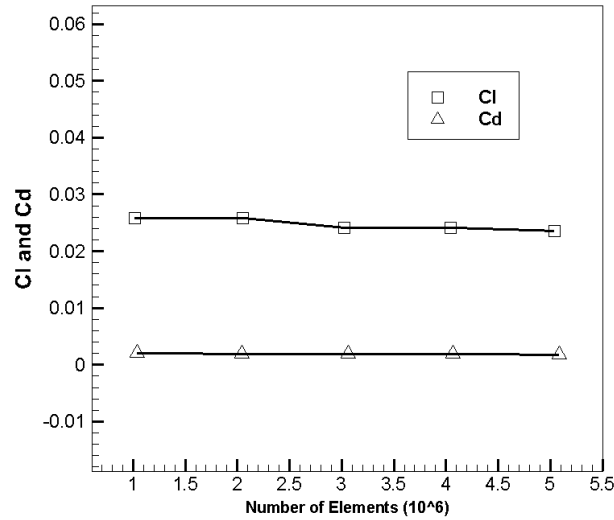


Fig. 3 Grid independence study for Cl and Cd convergence

Table 2 Flow conditions of Onera M 6 wing used for validation

Parameter	Values
Mach number	0.8395
Angle of attack	3.06°
sideslip	0°
Reynolds number	11.72×10 <sup>6</sup>
Mean aerodynamic chord	0.646 m

case for external flow fields due to transonic flow complexities such as shock waves, flow separation, turbulent boundary layer, and simple geometry, Nambu *et al.* (2015). Onera M6 is a semi-span untwisted wing with 30° swept with the application of a symmetric airfoil in the ONERA D section. The flow conditions used for validation are tabulated in Table 2 and are sourced from Schmitt et Charpin (1979).

The bullet shape domain is the computational domain used for simulations. The mesh is composed of 3,37,759 tetrahedral elements with four boundary conditions such as Euler wall on the wing, pressure far-field on the far side, velocity inlet and pressure outlet, and symmetry near the wall, where half wing is attached. The pressure distribution, obtained from the simulations at four different spanwise locations, is compared with experimental results, and the outcomes are plotted in Fig. 4 (a)-(c). An overall agreement can be observed between the experimental and numerical results. Additionally, the shock wave is accurately predicted on the suction side of the wing. Overall, the pressure distribution from the aerodynamic solver, used for this research, agrees well with the experimental data of Onera M6. It correctly predicts the position and strength of the shock wave.

#### 4. Results

The simulation results for all three ‘flying V’ configurations have been discussed in this section

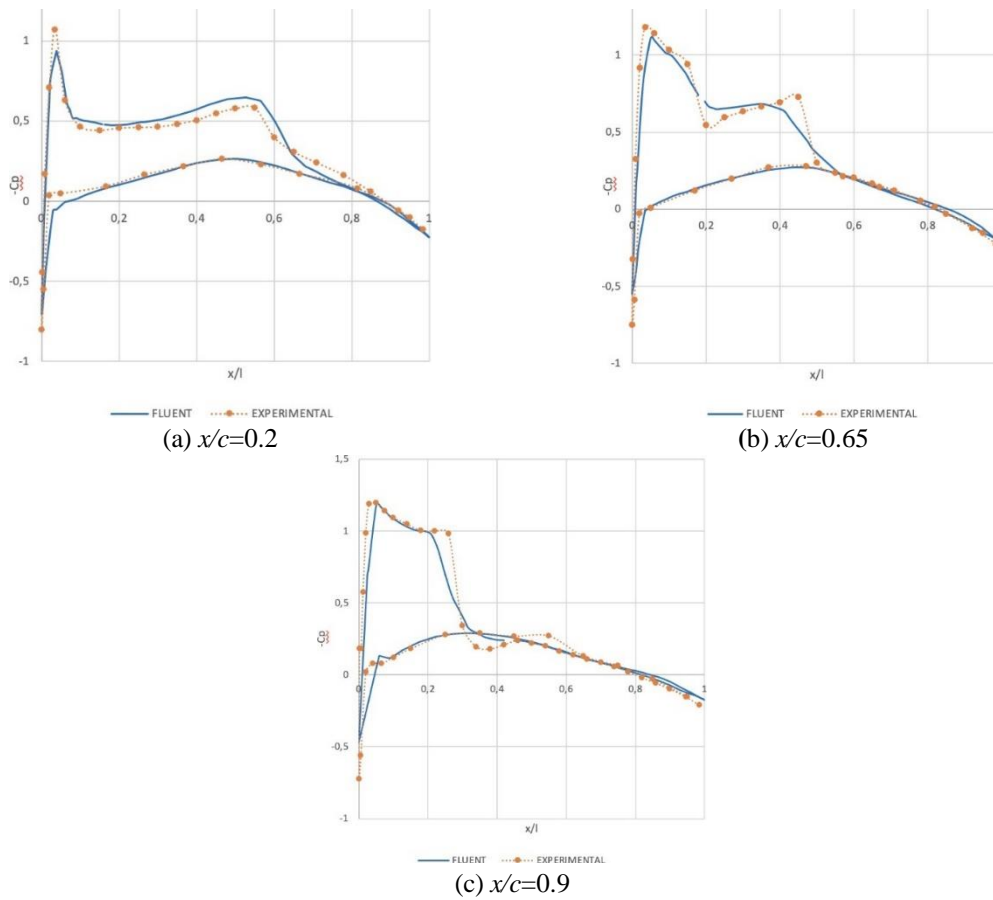


Fig. 4 Onera M6 wing: cp distribution at different span-wise locations

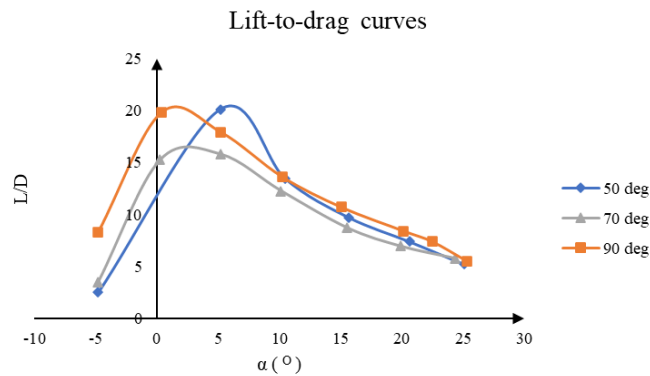


Fig. 5 Lift-to-drag ratio versus AoA curves for the three flying V configurations.

in terms of flow physics, aerodynamic coefficients' variations, streamlines, and pressure coefficients' distribution. All the results are obtained in the cruise phase with the cruise Mach number being 0.15.

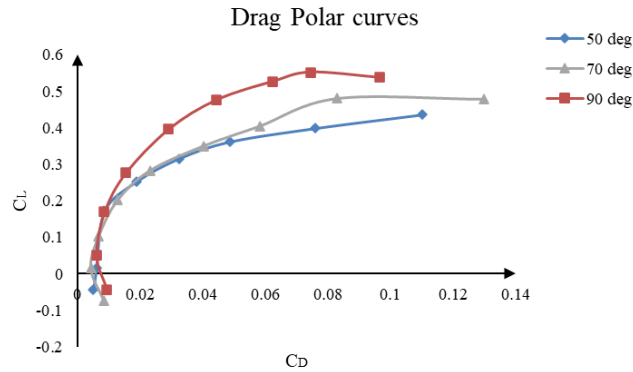


Fig. 6 Drag polar curves for the three flying V configurations.

Table 3 Comparison of aerodynamics results for different FW configurations

Aerodynamic parameter	V-angle 90°	V-angle 50°	V-angle 70°
Maximum lift coefficient	0.50	0.46	0.41
Stall angle	22°	35°	20°
The zero-lift angle of attack	-7°	-6°	-6°
Ideal-lift coefficient	0.12	0.04	0.06
The angle of attack corresponding to $C_{ld}$	-1°	-5°	-2°
Lift coefficient at zero angles of attack	0.18	0.1	0.1
Minimum drag coefficient	0.00766	0.00765	0.00583

#### 4.1 Comparison of results

Drag polar curves and Lift-to-drag ratio versus AoA curves for the three flying V configurations, 50 deg, 70 deg, and 90 deg are presented in Figs. 5 and 6 respectively.

Lift-to-drag ratio curves reveal that the 50° and 90° configuration has  $(L/D)_{\max}$  value of 20 obtained at AoA equal to 5° and 0° respectively. While the 70° configuration has  $(L/D)_{\max}$  value of 15 obtained at AoA equal to 0°. Among three flying V configurations, 90° geometry had the maximum lift coefficient (0.55). The value is 25% higher than the maximum lift for 70° geometry and 8% higher than 50° geometry. The 50° configuration was found to have a stall angle of 35°, compared to the 90° geometry with a stall angle of 22° and 70° geometry with a stall angle of 20°. For minimum drag, both 90° and 70° configurations had a similar value i.e., 0.0076, while for 50° geometry, it was 0.0052 with 31.58% less value, which resulted in reduced fuel consumption. A comparison among the three flying V configurations in terms of different aerodynamic parameters is tabulated in Table 3. To conclude, 90° geometry was found to be the best geometry compared to the other two main V- angles, in terms of lift coefficient.

#### 4.2 Angles of attack influence

The overall aerodynamics behavior, at a range of AoA for the main angle at 50° configuration is discussed. The pressure distribution reveals a conventional wing pressure behavior over the suction side of the ‘flying V’ main wing. The pressure reaches the maximum value at the

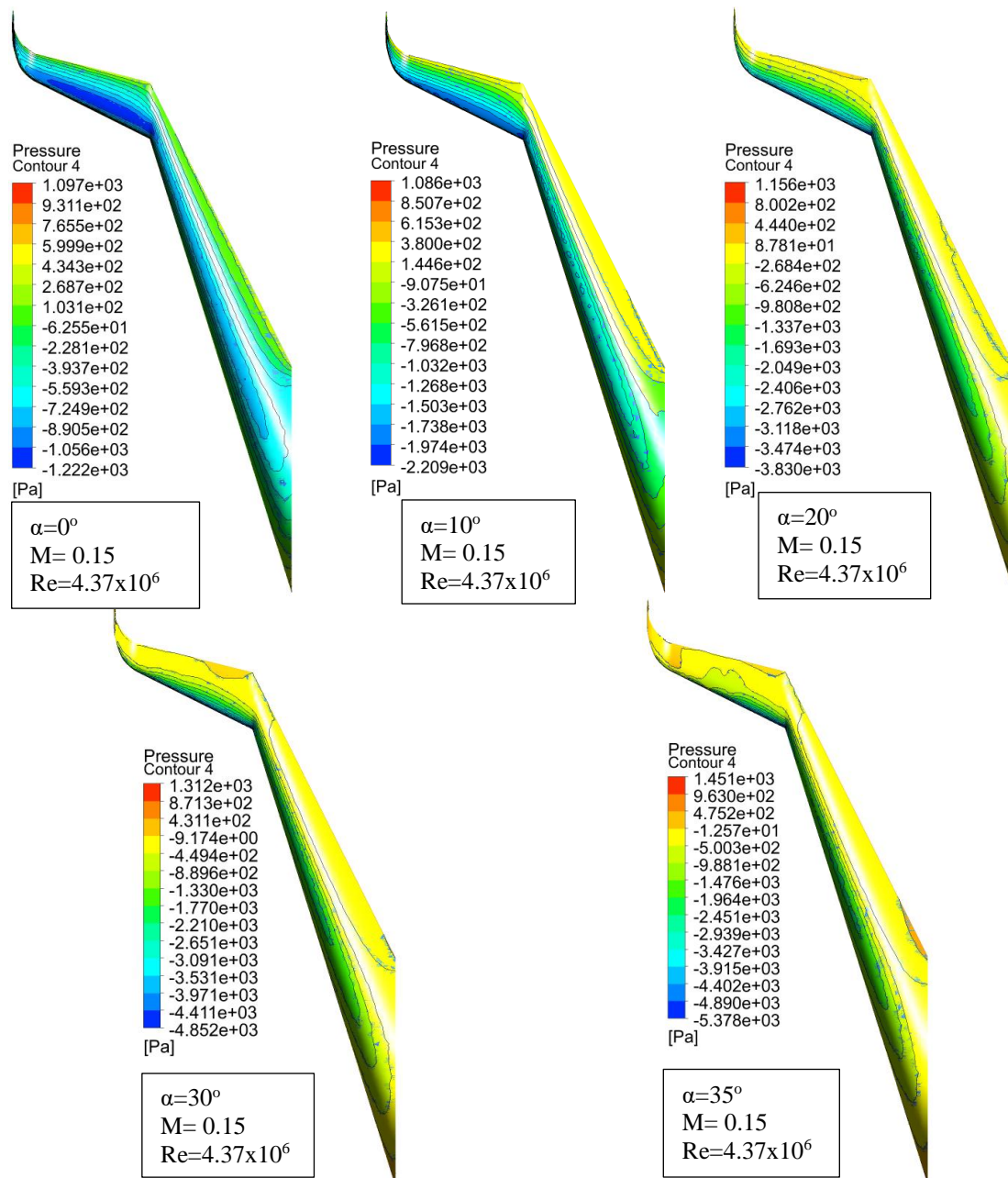


Fig. 7 Surface pressure distributions on the suction side of flying-V for main angle  $50^\circ$  configuration at AoA,  $0^\circ$ ,  $10^\circ$ ,  $20^\circ$ ,  $30^\circ$ , and  $35^\circ$ ,  $M=0.15$  and  $Re=4.37 \times 10^6$

stagnation point after which it gradually decreases and reaches the minimum pressure peak at the flow expansion zone over the wing leading edge. At  $\alpha=30^\circ$  and  $35^\circ$ , a negative pressure is evident over the whole suction side of the wing as shown in Fig. 7, except for a small region of positive pressure which indicates the onset of flow separation at the trailing edge, next to the wing root.

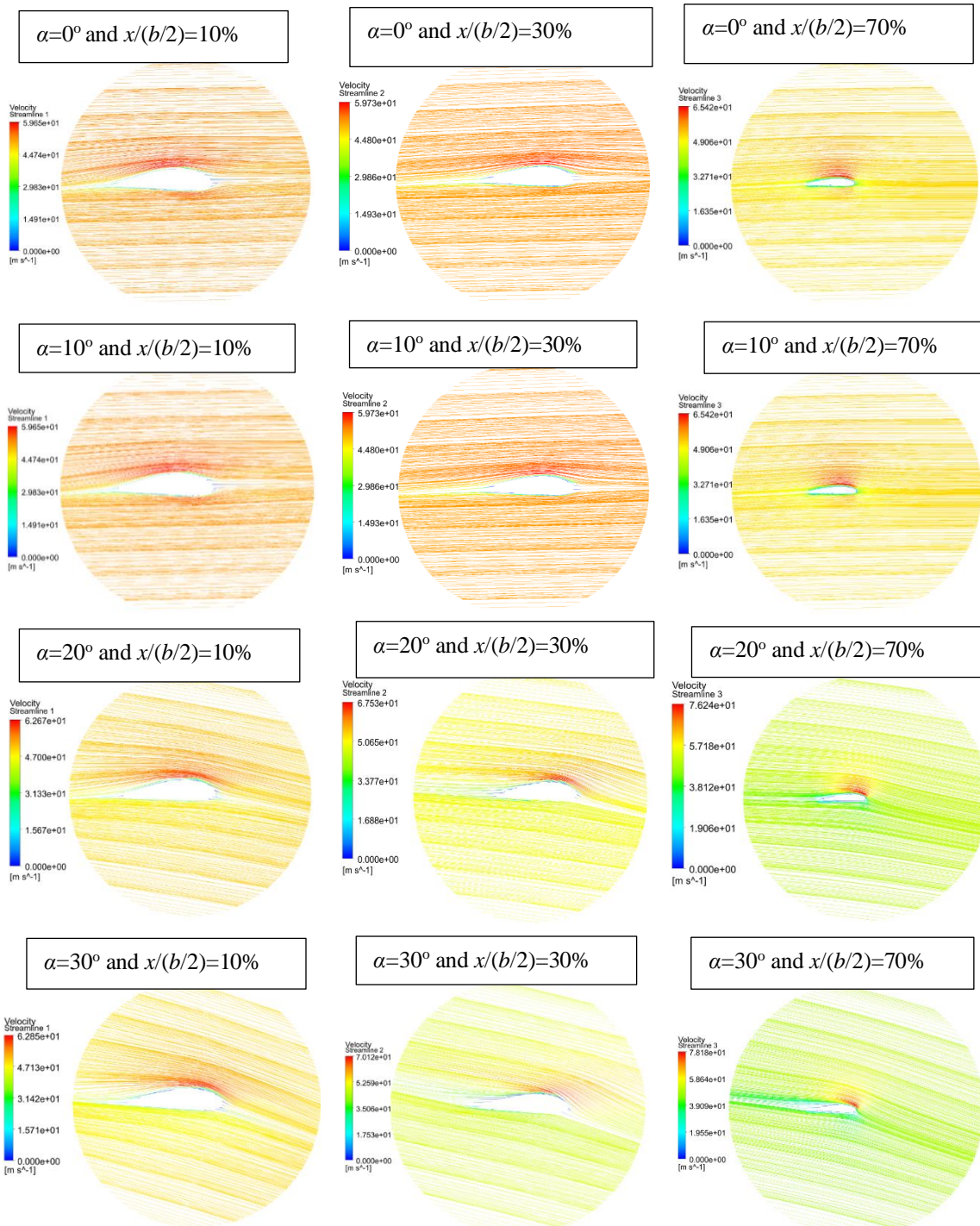


Fig. 8 Streamlines distributions for flying-V, main angle  $50^\circ$  configuration at AoA  $0^\circ$ ,  $10^\circ$ ,  $20^\circ$ ,  $30^\circ$  and  $35^\circ$  at  $x/(b/2)=10\%$ ,  $30\%$  and  $70\%$  spanwise locations and  $35^\circ$ ,  $M=0.15$  and  $Re=4.37 \times 10^6$

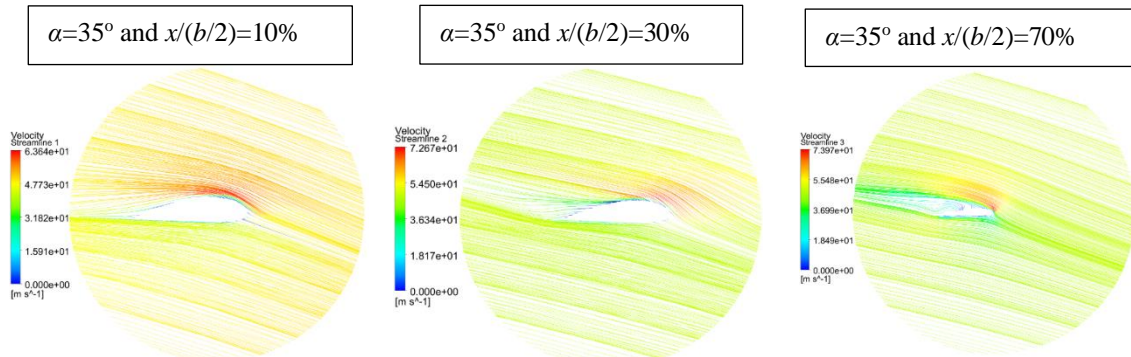


Fig. 8 Continued

This separation region grows in size and reaches 20% $c$  in diameter for  $\alpha=35^\circ$  with increasing angle of attack values. The trailing edge elevons and blended winglets have relatively higher positive pressure distribution that starts at the trailing edge and quickly spread across the whole elevon and winglet suction side areas. At  $\alpha=30^\circ$  and  $35^\circ$ , the separation region gets extended to include the leading edge as well as shown in Fig. 8. The above flow behavior is confirmed by the distribution of streamlines for flying V with a main angle equal to  $50^\circ$  at  $x/(b/2)=10\%$ ,  $30\%$ , and  $70\%$  spanwise positions at  $\alpha=30^\circ$  and  $35^\circ$  as shown in Fig. 9. even though the stall is delayed to  $\alpha=35^\circ$  for this configuration, at angles equal to and higher than  $30^\circ$ , the flying V possesses no sufficient lateral, longitudinal, and directional controls.

Fig. 8 illustrates the streamlines distribution at different AoAs over different span-wise locations that vary from root to tip. The flow is attached near the main wing root at  $x/(b/2)=10\%$  for all the ranges of AoA between  $0^\circ$  to  $35^\circ$ . The flow remains attached to the lower and upper surfaces of the main wing near the main wing mid-span at  $x/(b/2)=30\%$ . But at  $\alpha=20^\circ$  and  $30^\circ$ , the separation gets initiated as a small separation bubble at the suction side just near the maximum wing thickness point. At this point, drop inflow velocity is evident as can be observed in Fig. 8. At  $\alpha=35^\circ$  and  $x/(b/2)=30\%$ , the separation region gets extended over the whole suction side behind the point of maximum thickness. At trailing edge elevon, streamline distribution occurs at the spanwise location at  $x/(b/2)=70\%$  as depicted in Fig. 8. The flow is attached at the relatively low angles of attack spans between  $0^\circ$  and  $10^\circ$ . The onset of the separation is predicted at  $\alpha=20^\circ$  that gets extended over the entire suction side at  $\alpha=20^\circ$  and  $35^\circ$ .

Pressure distribution for the main angle  $90^\circ$  configuration versus the angle of AoA shows the same distribution of pressure contours trend over suction-side alike  $50^\circ$  configuration. Earlier separation was observed at a wider-trailing edge area for the main wing with a positive pressure bubble at the rear part of trailing-edge elevon at  $\alpha=15^\circ$ , which can be observed in Fig. 9. Similar pressure distributions are shown for  $\alpha=20^\circ$  which indicates that there is a relatively earlier loss of lift and onset for a stall at  $\alpha=22^\circ$  as shown in Fig. 9.

Streamline distributions, close to the main-wing root, remain attached for the range of  $\alpha=0^\circ$  to  $20^\circ$  as shown in Fig. 10 (left). Velocity loss, at the mid-section of the main wing, starts at  $\alpha=15^\circ$  as illustrated in Fig. 10 (middle). In contrast to the trailing edge, elevon separation is evident at  $\alpha=10^\circ$  with increasing in-depth at  $\alpha=15^\circ$  and  $\alpha=20^\circ$ . This flow behavior reemphasizes the fact that the control issue at angles of attacks is lesser for Flying V than the stall angle value.

However, coefficients negative values of the near-root and mid-span of the main wing pressure

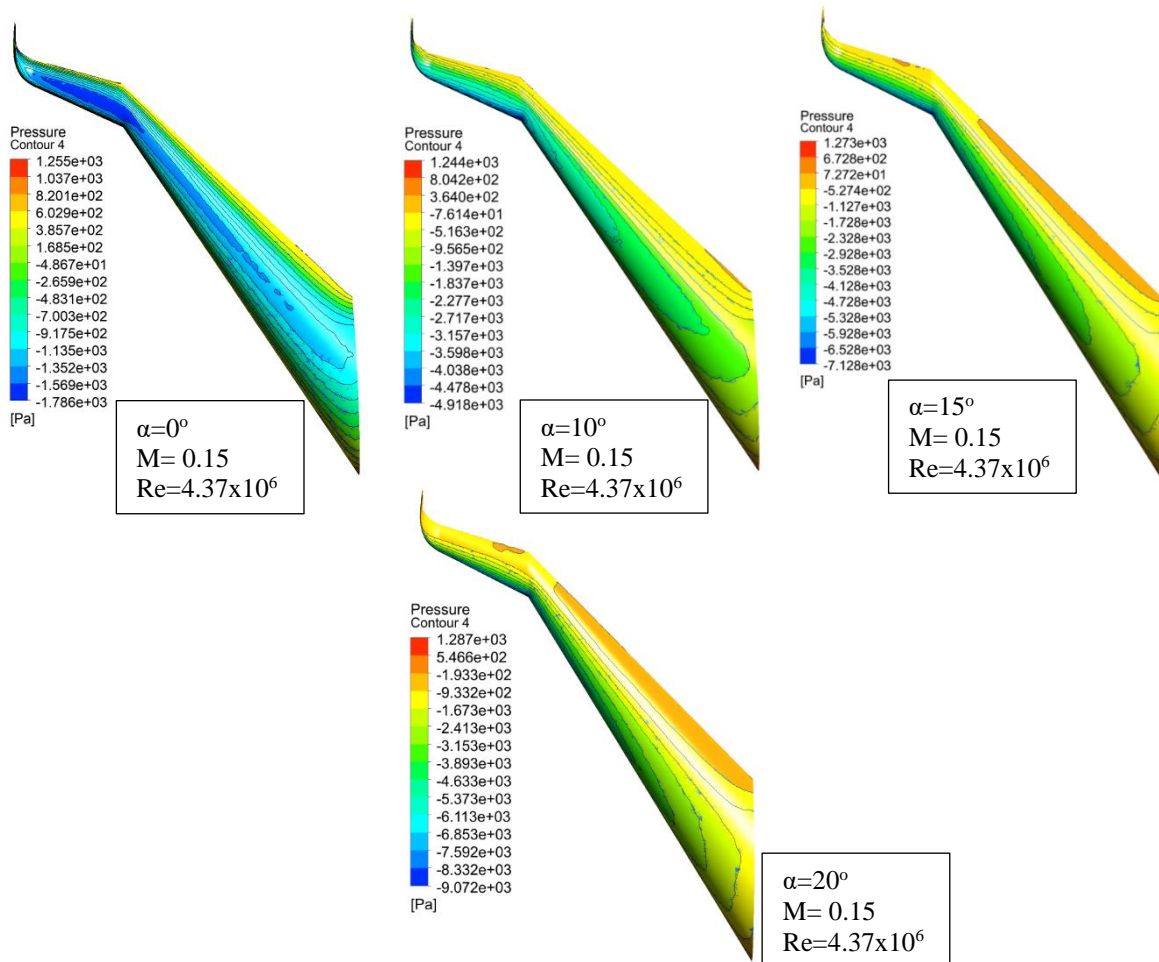


Fig. 9 Surface pressure distributions on the suction side of flying-V for main angle  $90^\circ$  configuration at AoA  $0^\circ$ ,  $10^\circ$ ,  $15^\circ$ , and  $20^\circ$ ,  $M=0.15$  and  $Re=4.37 \times 10^6$ .

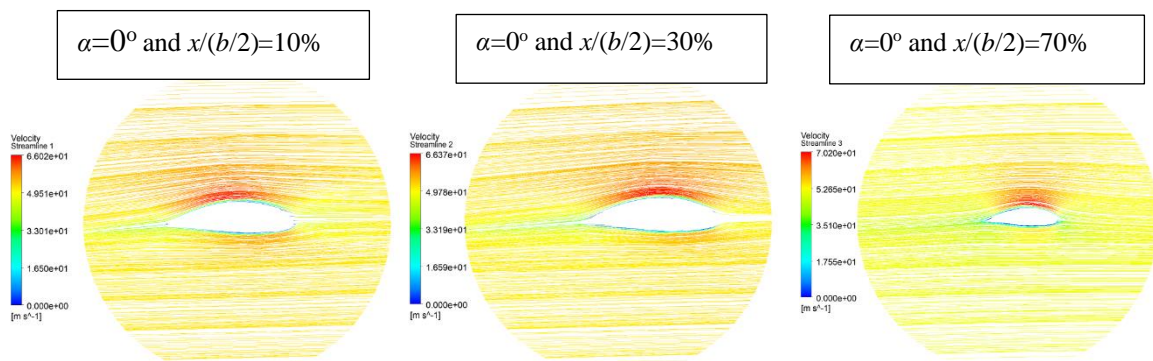


Fig. 10 Streamline distributions for flying-V, main angle  $90^\circ$  configuration at AoA  $0^\circ$ ,  $10^\circ$ ,  $15^\circ$  and  $20^\circ$  at  $x/(b/2)=10\%$ ,  $30\%$  and  $70\%$  spanwise locations at  $M=0.15$  and  $Re=4.37 \times 10^6$

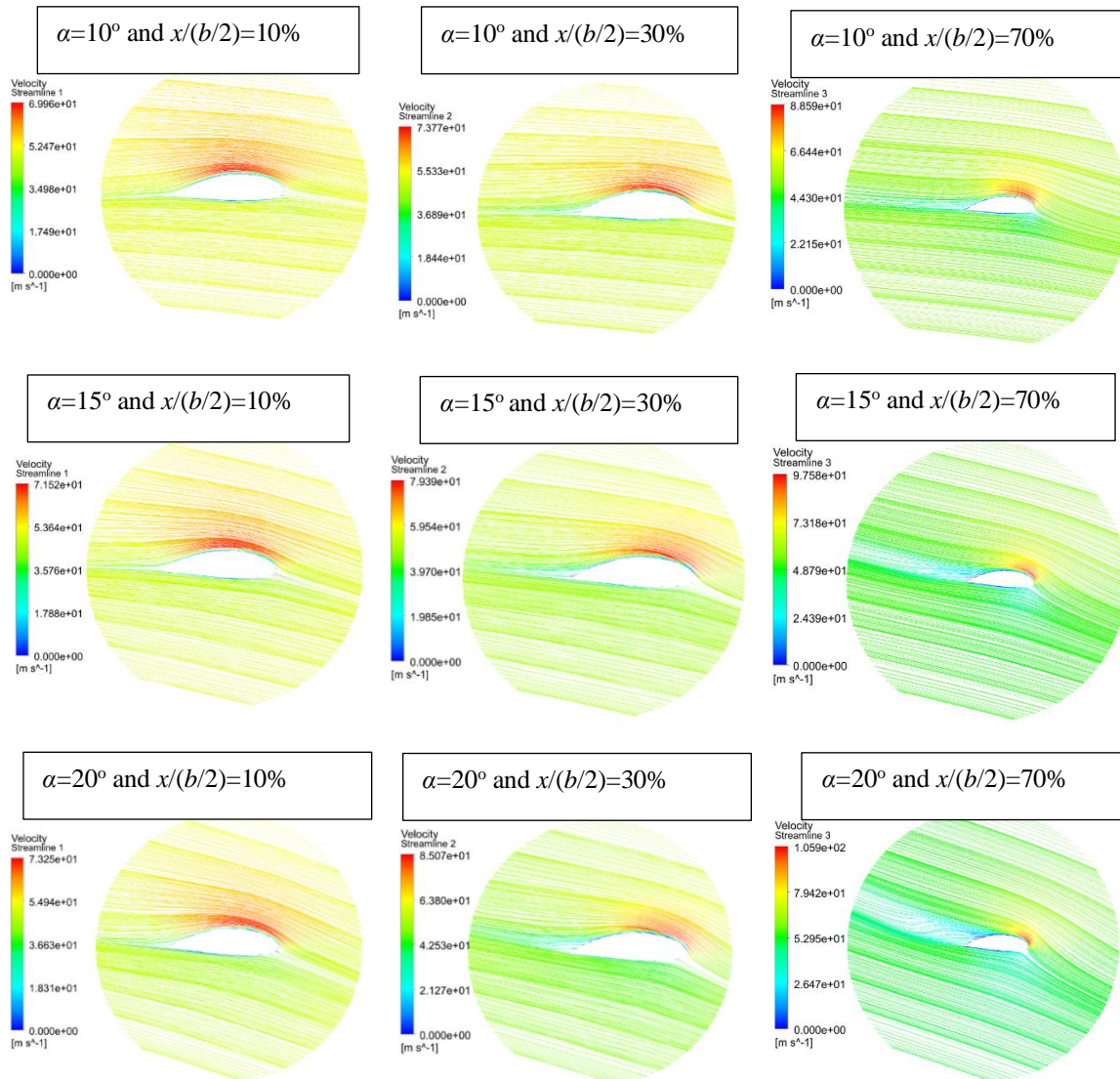


Fig. 10 Continued

coefficient increase with an increase in AoA.

#### 4.3 Angle of attack Influence

The distribution of the pressure coefficient follows a conventionally expected trend as the area enclosed increases with an increase in the angle of attack. Nevertheless, a decrease in peak negative pressure coefficient values is denoted by the pressure coefficient distributions, at the trailing edge of elevon when  $\alpha = 40^\circ$  and  $30^\circ$  for  $50^\circ$  and  $90^\circ$  flying V configurations respectively. These values are shown in Fig. 11(c) and Fig. 12(c). This phenomenon gets reflected in a smaller force that got generated at the elevon surface. Further, it also agrees with the stability issue

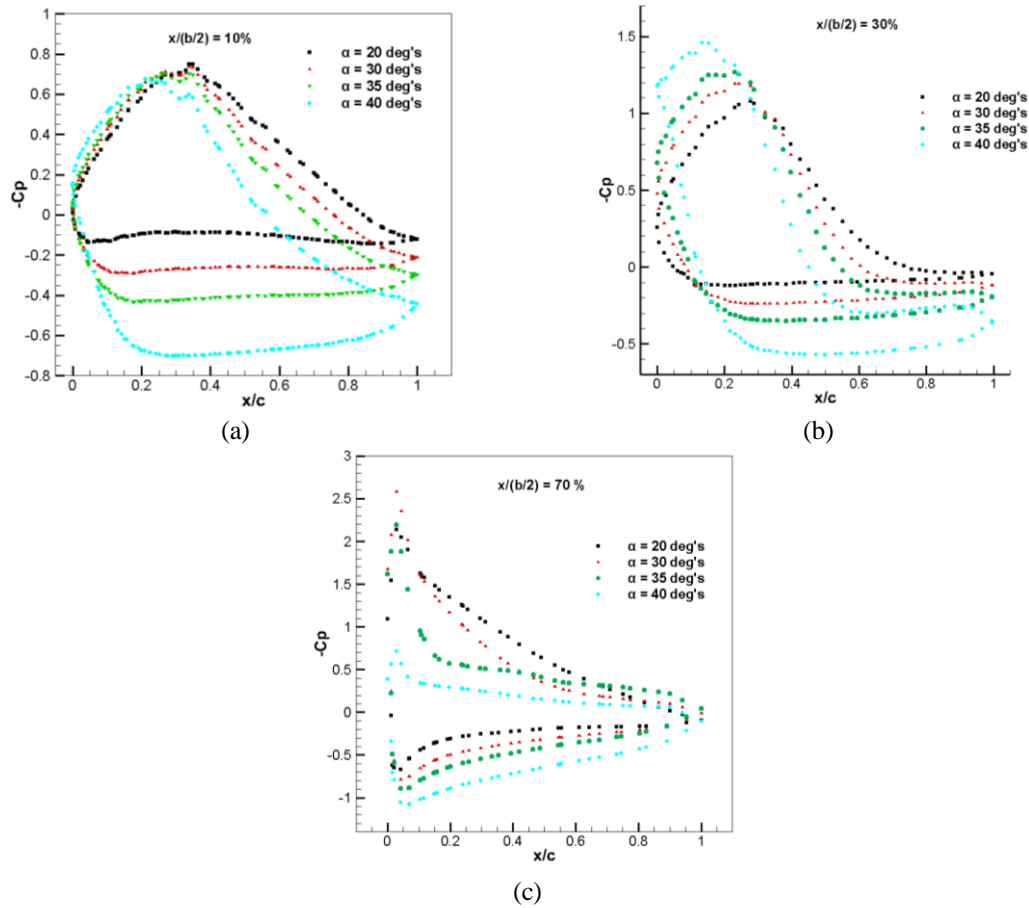


Fig. 11 Influence of AoA change on  $C_p$  distributions at  $x/(b/2)$ , (a) =10% (b) =30% and (c) =70% spanwise positions for flying-V, main angle  $50^\circ$  configuration,  $M=0.15$  and  $Re=4.37 \times 10^6$

previously reported at relatively higher angles.

## 5. Conclusions

Conventional aeronautical transport has grown leaps and bounds in the past few decades. However, it is also expected to grow in multiple numbers in the near future. This scenario causes a significant environmental effect and noise emission. The typical fuselage-wing design has highly evolved and developed from its invention. Consequently, researchers and manufacturers have also investigated alternative designs such as flying wings and blended wing bodies. The research conducted on recent geometry has demonstrated to be more efficient than a conventional tube and wings aircraft. The current research work numerically investigated the effects of main V-angles on aerodynamic performance. Three configurations were selected with three different main V-angles such as  $50^\circ$ ,  $70^\circ$ , and  $90^\circ$  representing minimum, moderate, and maximum V-angle configurations respectively. The results obtained reveal that  $90^\circ$  geometry had the maximum lift coefficient of

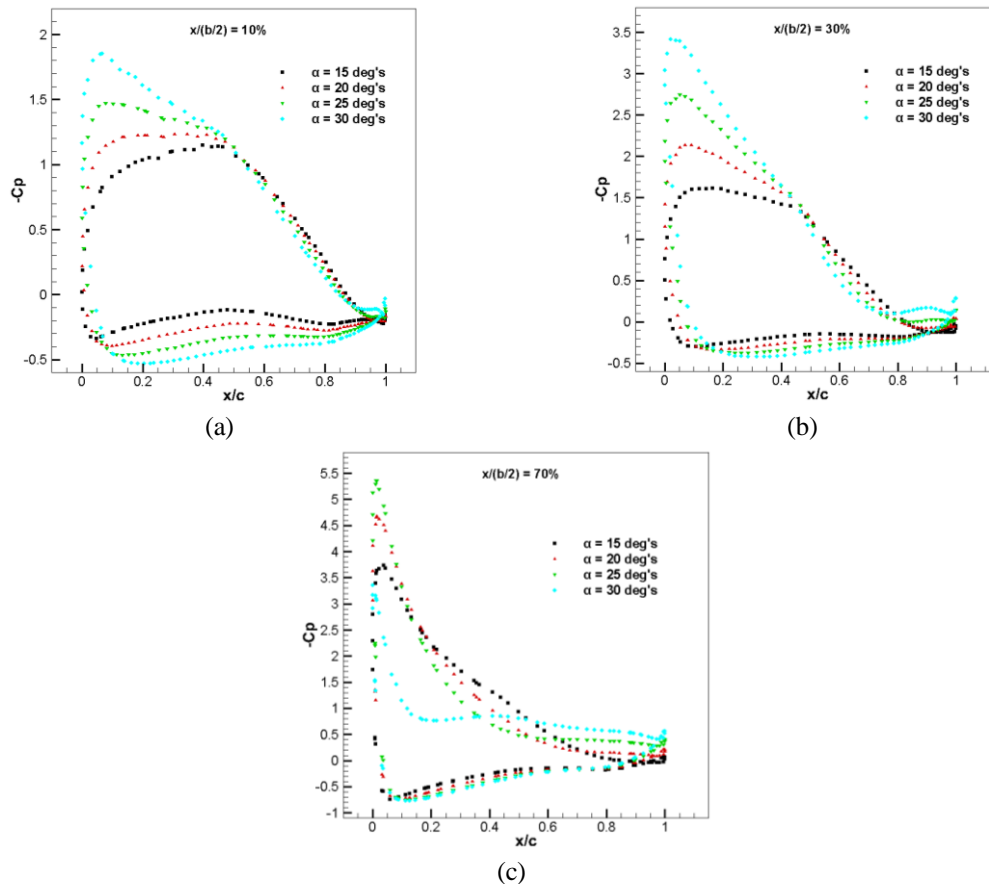


Fig. 12 Influence of AoA change on  $C_p$  distributions at  $x/(b/2)$ , (a) =10% (b) =30% and (c) =70% spanwise positions for flying-V, main angle  $90^\circ$  configuration,  $M=0.15$  and  $Re=4.37 \times 10^6$

0.46, and a maximum lift-to-drag ratio of 20 obtained at AoA equal to  $0^\circ$  compared to other configurations. The ideal lift coefficient was the highest for  $90^\circ$  geometry (0.12). The minimum drag value showed no noticeable change for the three configurations with the value of 0.0076. Although flying V possesses significant aerodynamic and structural advantages, its stability and control issues must be attempted carefully and can be a subject of further research.

## References

- Ankith John Santosh, A. (2020), "Numerical investigation of the influence of ground effect on the FV aircraft: Influence of ground effect on the flying V aircraft", Master Thesis, TU Delft Library.
- Benad J. (2015), "Design of a commercial aircraft for high-subsonic speed as a flying wing 345 configuration", Technical Report, Airbus, Berlin.
- Bolsunovsky, A.L., Buzoverya, N.P., Gurevich, B.I., Denisov, V.E., Dunaevsky, A.I., Shkadov, L.M., ... & Zhurihin, J.P. (2001), "Flying wing-problems and decisions", *Aircraft Des.*, **4**(4), 193-219. [https://doi.org/10.1016/S1369-8869\(01\)00005-2](https://doi.org/10.1016/S1369-8869(01)00005-2).

- Chan, W. (2002), "The overgrid interface for computational simulations on overset grids", *32nd AIAA Fluid Dynamics Conference and Exhibit*, 3188.
- Faggiano, F., Vos, R., Baan, M. and Van Dijk, R. (2017), "Aerodynamic design of a flying V aircraft", *17th AIAA Aviation Technology, Integration, and Operations Conference*, 3589.
- Gebauer, J. and Benad, J. (2021), "Flying V and reference aircraft evacuation simulation and comparison", arXiv preprint arXiv:2102.06502.
- He, S., Guo, S., Liu, Y. and Luo, W. (2021), "Passive gust alleviation of a flying-wing aircraft by analysis and wind-tunnel test of a scaled model in dynamic similarity", *Aerosp. Sci. Technol.*, **113**, 106689. <https://doi.org/10.1016/j.ast.2021.106689>.
- Martinez-Val, R. (2007), "Flying wings. A new paradigm for civil aviation?", *Acta Polytechnica*, **47**(1), 1. <https://doi.org/10.14311/914>.
- Martinez-Val, R., Palacin, J.F. and Perez, E. (2008), "The evolution of jet airliners explained through the range equation", *Proc. Inst. Mech. Eng., Part G: J. Aerosp. Eng.*, **222**(6), 915-919. <https://doi.org/10.1243/09544100JAERO338>.
- Martinez-Val, R., Perez, E., Alfaro, P. and Perez, J. (2007), "Conceptual design of a medium size flying wing", *Proc. Inst. Mech. Eng., Part G: J. Aerosp. Eng.*, **221**(1), 57-66. <https://doi.org/10.1243/09544100JAERO9>.
- Martinez-Val, R., Perez, E., Puertas, J. and Roa, J. (2010), "Optimization of planform and cruise conditions of a transport flying wing", *Proc. Inst. Mech. Eng., Part G: J. Aerosp. Eng.*, **224**(12), 1243-1251. <https://doi.org/10.1243/09544100JAERO812>.
- Meng, C., Kaihua, Y. and Haibo, H. (2020, November), "Static aeroelastic effects on rudder efficiency of flying wing aircraft", *2020 3rd International Conference on Unmanned Systems (ICUS)*, 727-732.
- Nambu, T., Hashimoto, A., Aoyama, T. and Sato, T. (2015), "Numerical analysis of the ONERA-M6 wing with wind tunnel wall interference", *Trans. JPN Soc. Aeronaut. Space Sci.*, **58**(1), 7-14. <https://doi.org/10.2322/tjsass.58.7>.
- Oosterom, W. and Vos, R. (2022), "Conceptual design of a flying-V aircraft family", *AIAA AVIATION 2022 Forum*, 3200.
- Rubio Pascual, B. (2018), *Engine-Airframe Integration for the Flying-V*.
- Rubio Pascual, B. and Vos, R. (2020), "The effect of engine location on the aerodynamic efficiency of a flying-v aircraft", *AIAA Scitech 2020 Forum*, 1954.
- Sadraey, M.H. (2012), *Aircraft Design: A Systems Engineering Approach*, John Wiley & Sons.
- Schmitt, V. (1979), "Pressure distributions on the ONERA M6-wing at transonic Mach numbers, experimental data base for computer program assessment", *AGARD AR-138*.
- Syed, A.A., Moshtaghzadeh, M., Hodges, D.H. and Mardanpour, P. (2022), "Aeroelasticity of flying-wing aircraft subject to morphing: A stability study", *AIAA J.*, **60**(9), 5372-5385. <https://doi.org/10.2514/1.J061574>.
- Torenbeek, E. (2007), "Blended-wing-body and all wing airliners", *8th European Workshop on Aircraft Design Education*, May.
- Torenbeek, E. (2013), *Synthesis of Subsonic Airplane Design: An Introduction to the Preliminary Design of Subsonic General Aviation and Transport Aircraft, with Emphasis on Layout, Aerodynamic Design, Propulsion and Performance*, Springer Science & Business Media.
- Vassberg, J., Dehaan, M., Rivers, M. and Wahls, R. (2008, August), "Development of a common research model for applied CFD validation studies", *26th AIAA Applied Aerodynamics Conference*, 6919.
- Vink, P., Rotte, T., Anjani, S., Percuoco, C. and Vos, R. (2020), "Towards a hybrid comfortable passenger cabin interior for the flying V aircraft", *Int. J. Aviat., Aeronaut. Aerosp.*, **7**(1), 1. <https://doi.org/10.15394/ijaaa.2020.1431>.
- Wei, C., Huang, J. and Song, L. (2022), "Study on a rapid aerodynamic optimization method of flying wing aircraft for conceptual design", *Int. J. Aerosp. Eng.*, **2022**, Article ID 5775355. <https://doi.org/10.1155/2022/5775355>.
- Zhao, Z., Luo, Z., Deng, X., Li, S., Zhang, J. and Liu, J. (2022), "Influences of trailing-edge synthetic jets on longitudinal aerodynamic characteristics of a flying wing aircraft", *Phys. Fluid.*, **34**(12), 127115.

<https://doi.org/10.1063/5.0132080>.

Zhu, J., Shi, Z., Geng, X., Fu, J., Chen, S. and Chen, Y. (2022), "Vortex breakdown characteristics of flying wing aircraft based on jet flow control", *Phys. Fluid.*, **34**(2), 025112. <https://doi.org/10.1063/5.0076173>.

CC

## Nomenclature

$C_{Lmax}$	Maximum lift coefficient
$c_l$	Lift coefficient
$c_d$	Drag coefficient
$c_{ld}$	Design lift coefficient, it is chosen such that the flow hits the airfoil exactly parallel to the start of the camber line.
$C_m$	Moment coefficient
$t/c$	Thickness to chord ratio
$l$	Length scale equal to wingspan
$\alpha$	Angle of attack
$x$	Distance in x-axis direction
$b$	Wingspan length
$M$	Mach number
$c$	Chord length
$C_p$	Pressure coefficient
$K$	turbulent kinetic energy
$\omega$	specific turbulent dissipation rate

## Abbreviations

$AoA$	Angle of attack
<i>B-47</i>	Boeing B-47 Stratojet aircraft
<i>Flying V</i>	Modified FW, manufactured in cooperation with Future Project Office at Airbus.
<i>FW</i>	Flying wing
<i>ICEM</i>	Software package which provides advanced geometry/mesh generation
<i>Onera M6 wing</i>	Created in the 70s, it serves as a reference to validate CFD methods
<i>SST</i>	Shear stress transport